(9)

SPIE.

PROCEEDINGS OF SPIE VOLUME 9444

# INTERNATIONAL SEMINAR ON PHOTONICS, OPTICS, AND ITS APPLICATIONS (ISPHOA 2014)

14-15 October 2014
Sanur, Bali, Indonesia

*Editor*
**Aulia Nasution**

*Organized by*

Department of Engineering Physics – FTI

Institut Teknologi Sepuluh Nopember (Indonesia)

*Sponsored by*

The Optical Society (United States)

PT Telekomunikasi Selular (Indonesia)

PT Len Industri (Indonesia)

PT Sigma Cipta Caraka (Indonesia)

PROCEEDINGS OF SPIE

# *International Seminar on Photonics, Optics, and Its Applications (ISPhOA 2014)*

**Aulia Nasution**
*Editor*

**14–15 October 2014**
**Sanur, Bali, Indonesia**

*Organized by*
Department of Engineering Physics – FTI
Institut Teknologi Sepuluh Nopember (Indonesia)

*Sponsored by*
The Optical Society (United States)
PT Telekomunikasi Selular (Indonesia)
PT Len Industri (Indonesia)
PT Sigma Cipta Caraka (Indonesia)

*Published by*
SPIE

**Volume 9444**

The papers included in this volume were part of the technical conference cited on the cover and title page. Papers were selected and subject to review by the editors and conference program committee. Some conference presentations may not be available for publication. The papers published in these proceedings reflect the work and thoughts of the authors and are published herein as submitted. The publisher is not responsible for the validity of the information or for any outcomes resulting from reliance thereon.

Please use the following format to cite material from this book:
Author(s), "Title of Paper," in *International Seminar on Photonics, Optics, and Its Applications (ISPhOA 2014)*, edited by Aulia Nasution, Proceedings of SPIE Vol. 9444 (SPIE, Bellingham, WA, 2015) Article CID Number.

ISSN: 0277-786X
ISBN: 9781628415599

Published by
**SPIE**
P.O. Box 10, Bellingham, Washington 98227-0010 USA
Telephone +1 360 676 3290 (Pacific Time) · Fax +1 360 647 1445
SPIE.org

Copyright © 2015, Society of Photo-Optical Instrumentation Engineers.

Copying of material in this book for internal or personal use, or for the internal or personal use of specific clients, beyond the fair use provisions granted by the U.S. Copyright Law is authorized by SPIE subject to payment of copying fees. The Transactional Reporting Service base fee for this volume is $18.00 per article (or portion thereof), which should be paid directly to the Copyright Clearance Center (CCC), 222 Rosewood Drive, Danvers, MA 01923. Payment may also be made electronically through CCC Online at copyright.com. Other copying for republication, resale, advertising or promotion, or any form of systematic or multiple reproduction of any material in this book is prohibited except with permission in writing from the publisher. The CCC fee code is 0277-786X/15/$18.00.

Printed in the United States of America.

Publication of record for individual papers is online in the SPIE Digital Library.

SPIE Digital Library
SPIEDigitalLibrary.org

---

**Paper Numbering:** Proceedings of SPIE follow an e-First publication model, with papers published first online and then in print. Papers are published as they are submitted and meet publication criteria. A unique citation identifier (CID) number is assigned to each article at the time of the first publication. Utilization of CIDs allows articles to be fully citable as soon as they are published online, and connects the same identifier to all online, print, and electronic versions of the publication. SPIE uses a six-digit CID article numbering system in which:

- The first four digits correspond to the SPIE volume number.
- The last two digits indicate publication order within the volume using a Base 36 numbering system employing both numerals and letters. These two-number sets start with 00, 01, 02, 03, 04, 05, 06, 07, 08, 09, 0A, 0B ... 0Z, followed by 10-1Z, 20-2Z, etc.

The CID Number appears on each page of the manuscript. The complete citation is used on the first page, and an abbreviated version on subsequent pages.

# Contents


vii *Authors*

ix *Conference Committee*

xi *Introduction*

xiii *Sponsors*

**INVITED SESSION**

9444 02 **Compact one-lens fluorescence microscope using CMOS image sensor (Invited Paper)** [9444-21]

9444 03 **Semiconductor lasers for versatile applications from global communications to on-chip interconnects (Invited Paper)** [9444-65]

9444 04 **Rigorous characterization of photonic devices by finite element method (Invited Paper)** [9444-66]

9444 05 **Photonics engineering: snapshot applications in healthcare, homeland security, agriculture, and industry (Invited Paper)** [9444-67]

9444 06 **Identifying the best chalcogenide glass compositions for the application in mid-infrared waveguides (Invited Paper)** [9444-10]

**PHOTONICS AND OPTICS APPLICATIONS**

9444 07 **Large ring laser gyroscopes: towards absolute rotation rate sensing** [9444-62]

9444 08 **TOPAS-based humidity insensitive polymer planar Bragg gratings for temperature and multi-axial strain sensing** [9444-19]

9444 09 **Activating neurons by light in free-moving adult flies** [9444-4]

9444 0A **Liquid level sensing based on laser differential confocal detectors** [9444-16]

9444 0B **Evaluating compact SAR polarimetry for tropical forest monitoring** [9444-35]

9444 0C **Interferometric processing of C-band SAR data for the improvement of stand age estimation in rubber plantation** [9444-9]

9444 0D **Radial line method for rear-view mirror distortion detection** [9444-49]

9444 0E **Design of low cost smart infusion device** [9444-43]

9444 0F **Tapered fiber optic sensor for potassium detection in distilled water** [9444-60]

9444 0G **Web camera as low cost multispectral sensor for quantification of chlorophyll in soybean leaves** [9444-50]

9444 0H **Mapping system for the surface temperature in the Ijen Crater by Landsat-8 imagery with supervised image segmentation method based on fuzzy logic** [9444-55]

## PHOTONICS MATERIALS

9444 0I **Fundamental and harmonic soliton mode-locked erbium-doped fiber laser using single-walled carbon nanotubes embedded in poly (ethylene oxide) film saturable absorber** [9444-26]

9444 0J **Polarization dependent terahertz generation efficiency by optical rectification in $LiNbO_3$** [9444-31]

9444 0K **Al-doped MgZnO/p-AlGaN heterojunction and their application in ultraviolet photodetectors** [9444-11]

9444 0L **Fabrication and characterization of cuprous oxide solar cell with net-shaped counter electrode** [9444-36]

9444 0M **The effect of spectrum range limitation to the efficiency of $Al_{0.3}Ga_{0.7}As/GaAs/InP/Ge$ multijunction solar cells: a simulation case** [9444-44]

9444 0N **Spectral calibration of the coded aperture spectra imaging system** [9444-8]

9444 0O **Co-sensitized natural dyes potentially used to enhance light harvesting capability** [9444-46]

9444 0P **Identify paraffin-embedded brain glioma using terahertz pulsed spectroscopy** [9444-32]

9444 0Q **Modeling and experiment of dye-sensitized solar cell with vertically aligned ZnO nanorods through chemical bath deposition** [9444-51]

9444 0R **Mechanical and optical characterization of bio-nanocomposite from pineapple leaf fiber material for food packaging** [9444-53]

## PHOTONICS DEVICE DEVELOPMENTS

9444 0S **Fabrication of 1D photonic crystal by sol-gel method for tuning the emission of CdSe colloidal quantum dot** [9444-30]

9444 0T **Optical response characteristics of strained uniform fiber Bragg grating using laser diode** [9444-42]

9444 0U **Phase matching analyses of anti-Stokes pulses with four wave mixing in birefringence photonic crystal fibers** [9444-37]

9444 0V **Using a telecommunication-grade single mode patchcord as an optical extensometer based on bending loss** [9444-17]

9444 0W **Load effect on an SMS fiber structure embedded in a high-density polyethylene** [9444-58]

9444 0X **Research on key technologies of high repetition rate optical frequency comb** [9444-15]

9444 0Y **Optical system design of the snapshot imaging spectrometer using image replication based on Wollaston prism** [9444-6]

9444 0Z **Preliminary design of land displacement-optical fiber sensor and analysis of observation during laboratory and field test** [9444-18]

9444 10 **SMS fiber structure with a multimode fiber graded index type for a temperature measurement using an intensity-based interrogation system** [9444-59]

9444 11 **Design of GaN-based S-bend Y-branch power splitter with MMI structure** [9444-41]

9444 12 **16-channel arrayed waveguide grating (AWG) demultiplexer design on SOI wafer for application in CWDM-PON** [9444-27]

9444 13 **Broadband millimeter-wave electro-optic modulator using multi patch antennas for pico-cell radar networks** [9444-28]

9444 14 **Local density of optical states of an asymmetric waveguide grating at photonic band gap resonant wavelength** [9444-5]

**POSTER SESSION**

9444 15 **A mid-IR optical emission spectrometer with a PbSe array detector for analyzing spectral characteristic of IR flares** [9444-29]

9444 16 **Colour harmony of two colour combinations in clothes matching** [9444-12]

9444 17 **Development of optical inspection system for detecting malfunctions of digital micromirror device** [9444-34]

# Local Density of Optical States of an Asymmetric Waveguide Grating at Photonic Band Gap Resonant Wavelength

Husin Alatas*, Tony I. Sumaryada, Faozan Ahmad
Photonics Research Group, Department of Physics, Bogor Agricultural University,
Jl. Meranti, Kampus IPB Darmaga, Bogor 16680, Indonesia

## ABSTRACT

We have investigated the characteristics of local density of optical states (LDOS) at photonic band gap resonant wavelength of an asymmetric waveguide grating based on Green's function formulation. It is found that the LDOS of the considered structure exhibits different characteristics in its localization between the upper and lower resonant wavelengths of the corresponding photonic band gap edges.

**Keywords:** Local density of optical states, waveguide grating, Green's function method, resonant state.

## 1. INTRODUCTION

In recent years, the asymmetric waveguide grating (WG) structure in the form of asymmetric corrugated slab waveguide has been intensively used in integrated optical device for sensor application [1]. The existence of photonic band gap (PBG) in an asymmetric WG, where light in certain range of wavelength cannot propagates, has been well studied [2]. The wavelength variation of resonant wavelengths at PBG edges are usually considered in sensor device due to its ability to detect the change of refractive index of the surrounding material.

Recently also, it was reported the characteristics of energy confinement, scattering loss and group velocity of asymmetric WG at resonant states of the corresponding PBG [3]. It was shown that for increasing number of teeth, the group velocity and energy confinement can be enhanced significantly without affecting the scattering loss on both upper and lower resonant states. In the meantime, groove depth variation exhibited different characteristics between both resonant states. It is well known that the number of teeth as well as groove depth that lead to the variation of the corresponding parameters affect significantly its sensitivity.

On the other hand, it is well known that one of the important properties of optical structure is its ability to accommodate photon eigenmodes at specific location inside the asymmetric WG. This property is represented by the so called local density of optical states or LDOS. There are several ways to calculate LDOS e.g. [4, 5, 6]. One of them is through Green's function method in the form of Dyson formulation [6]. In this method the corresponding LDOS can be calculated directly without calculating the electromagnetic field first as needed in the method given in ref. [4,5]. Unlike finite-difference scheme, this method does not need boundary condition.

Following the results of ref. [3], in this report we discuss the characteristics of LDOS of the associated asymmetric WG structure. Similar to that report, we employ the same Green's function method to calculate the related LDOS. We will discuss the dynamical characteristics of LDOS of the considered asymmetric WG with respect to the variation of number of teeth and groove depth showing the different behavior between the upper and lower resonant states.

## 2. ASYMMETRIC WAVEGUIDE GRATING STRUCTURE

We consider an asymmetric WG structure similar to what was discussed previously in ref. [3]. The corresponding structure is a three layer system consisting of a cladding with $n_{clad} = 1$, corrugated slab dielectric waveguide of thickness $h = 160\ nm$ with $n_{slab} = 1.98$, and substrate of $n_{sub} = 1.44$, while the grating period is set to $\Lambda = 200\ nm$. We consider the TE mode electric field illuminated from the left side. In this mode, the associated Green's function is a scalar function [6].

*alatas@ipb.ac.id

International Seminar on Photonics, Optics, and Its Applications (ISPhOA 2014), edited by Aulia Nasution,
Proc. of SPIE Vol. 9444, 944414 · © 2015 SPIE · CCC code: 0277-786X/15/$18 · doi: 10.1117/12.2074195

Given in Fig. 1 is the sketch of corresponding asymmetric WG in which the corrugated section is only at one side of the slab waveguide. Here, we denote the number of teeth by $N$ and $g$ for the groove depth as parameters to be varied.

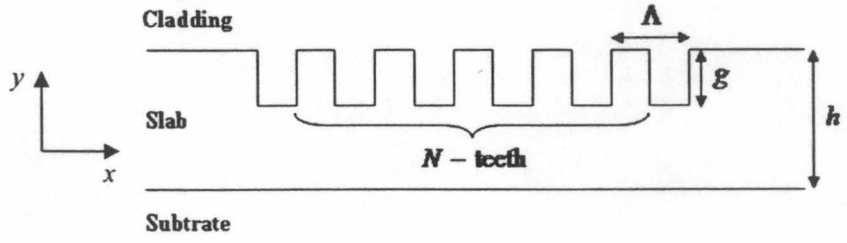


Fig. 1 Sketch of asymmetric waveguide grating

## 3. GREEN'S FUNCTION FORMULATION

We begin the calculation of Green's function $G(r,r')$ of the corresponding asymmetric WG by finding out the background Green's function $G^B(r,r')$, namely the Green's function of three layer system without corrugated section. The detailed calculation for this function can be found in ref. [6]. After constructing $G^B(r,r')$, the function $G(r,r')$ can then be calculated from the following equation:

$$G(r,r') = G^B(r,r') + \int_A G^B(r,r'')k_0^2\Delta\varepsilon(r'')G(r'',r')dA'' \tag{1}$$

Here $r=(x,y)$ and $r'=(x',y')$ denoting the observation point and dipole position respectively, while $\Delta\varepsilon$ representing the perturbation in the form of permittivity contrast between background and corrugated section. The symbol $k_0$ is the vacuum wavenumber, while $A$ is the computational domain. Having the Green's function (1) at hand, one can calculate it based on the following discrete form:

$$G_{ij} = G^B_{ij} + \sum_{i=1,j=1,i\neq k,j\neq k}^{P} G^B_{ik}k_0^2\Delta\varepsilon_k\Delta A_k G_{kj} + M_i k_0^2\Delta\varepsilon_i G_{ij} - L\frac{\Delta\varepsilon_i}{\varepsilon_B}G_{ij} \tag{2}$$

where $M$ and $L$ are parameters to handle singularity [6]. In principle, Eq. (2) can be solved iteratively namely by adding the perturbation one by one into the background structure. From this Green's function one can calculate the corresponding electric field as follows:

$$E(r) = E^B(r) + \int_A G(r,r')k_0^2\Delta\varepsilon(r')E^B(r')dr' \tag{3}$$

where $E^B(r)$ is the fundamental mode of the slab waveguide.

To calculate all these we define the computational domain as follows: the left and right boundaries in $x-$direction is $(x_l,x_r)=(0,8)\mu m$, while the bottom and top boundaries in $y-$direction $(y_b,y_t)=(-40,200)nm$. In the mean time the meshes are set to $\Delta x = 20\,nm$ and $\Delta y = 10\,nm$. All these computational parameters are similar to that used in ref. [3].

## 4. LDOS CHARACTERISTICS

After findings the function $G(r,r')$, we can now calculate the LDOS using the following dimensionless definition [3, 7]:

$$\rho(r) = \frac{\mathrm{Im}[G(r,r)]}{\mathrm{Im}[G^B(r,r)]} \tag{3}$$

This quantity describes the number of photon eigenmode available between $\lambda$ to $\lambda+d\lambda$ in specific position $r$, where $\lambda$ denotes wavelength.

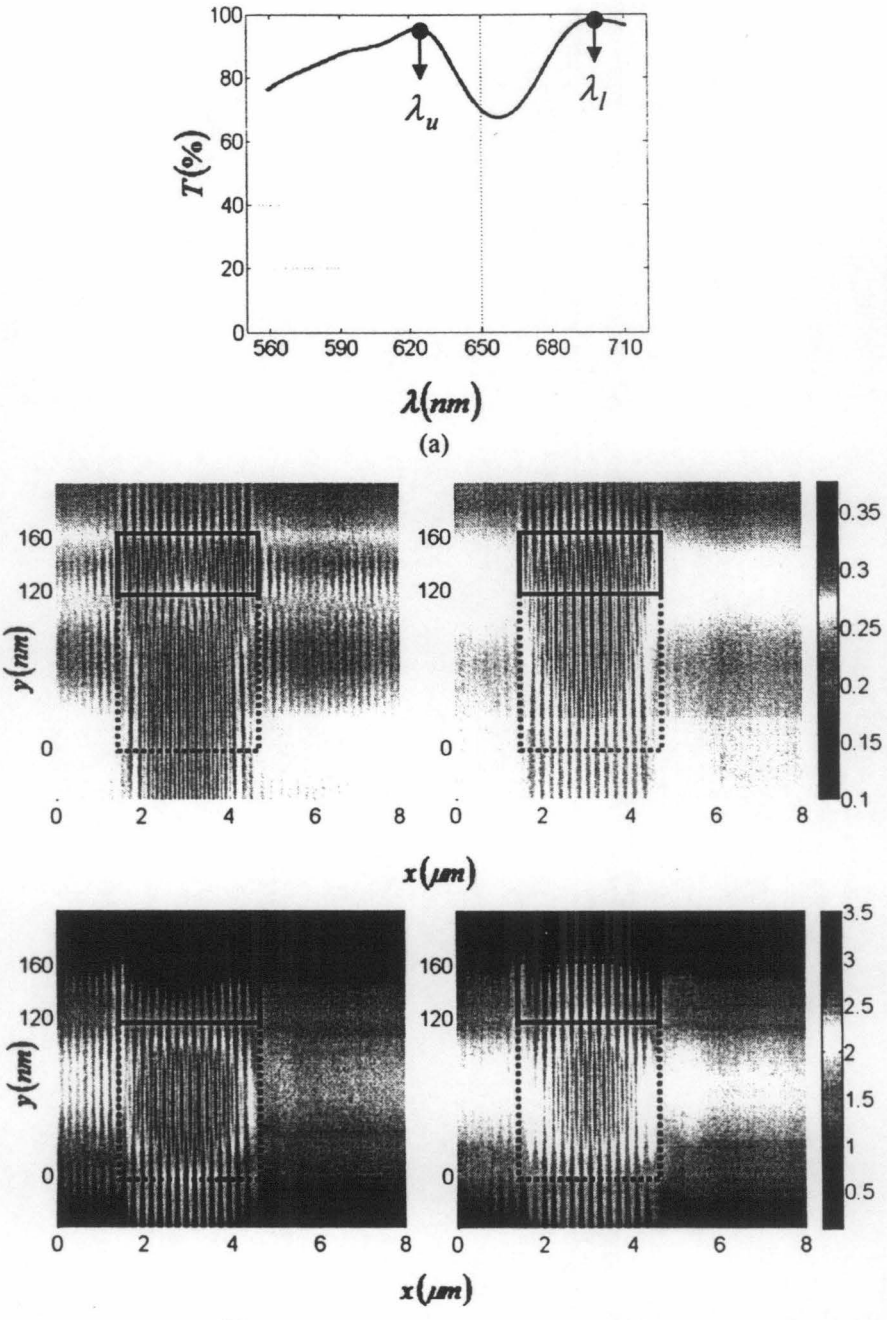


Fig. 2 (a) Transmittance of PBG of a specific asymmetric WG with $N = 14$ and $g = 40\ nm$. The left solid-dot denotes the upper resonant with shorter wavelength, while the right solid-dot represents the lower resonant with longer wavelength. (b) LDOS contour (top panel) at upper resonant with $\lambda_u = 624\ nm$ and (c) at lower resonant with $\lambda_l = 697\ nm$, with the corresponding electric field (bottom panel). Corrugated area is inside the box with solid-line boundary, while box with dotted-line boundary is the uncorrugated area.

Depicted in Fig. 2 is an example of PBG of a specific asymmetric WG structure discussed previously in ref. [3] with $N = 14$ and $g = 20\ nm$, along with upper and lower resonant wavelengths, and the corresponding LDOS which is the main focus of this discussion.

It is clearly shown in the figure that both resonant exhibit different characteristics. For the upper resonant, the LDOS is mostly localize in the uncorrugated area, while for the lower resonant the localization occurs both in uncorrugated as well as corrugated areas. This phenomenon is consistent with the fact that the related electric fields are also localized in more or less the same areas for both cases as shown in the figure.

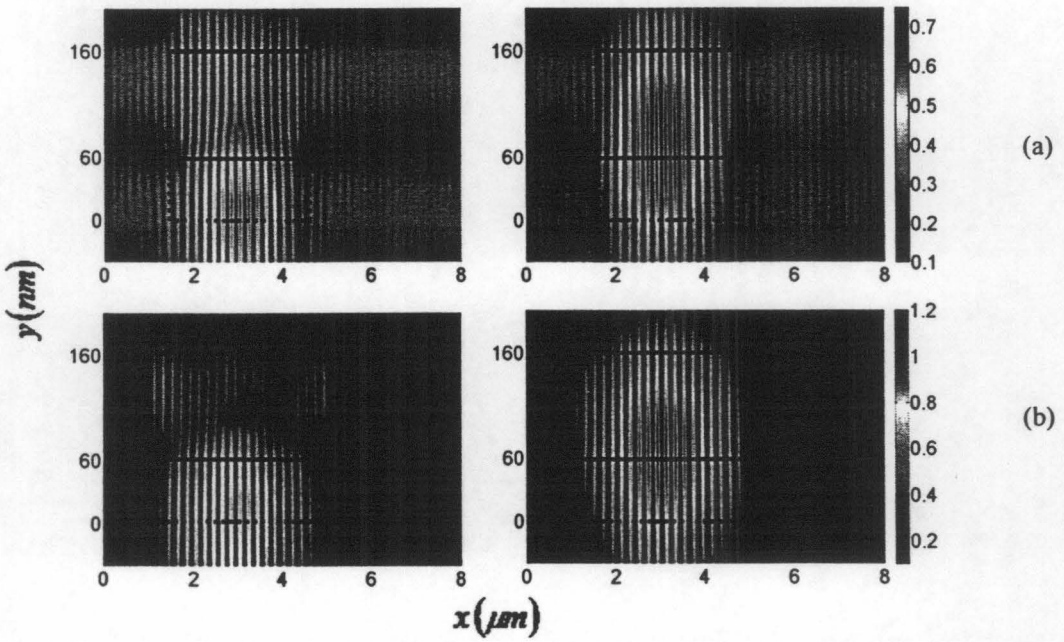


Fig. 3 LDOS contour of for upper (left panel) and lower (right panel) resonant for (a) $g = 100\ nm$ and $N = 14$, (b) for $g = 100\ nm$ and $N = 20$. Corrugated area is inside the box with solid-line boundary, while box with dotted-line boundary is the uncorrugated area.

The effect of groove depth on LDOS is shown in Fig. 3a for $g = 100\ nm$ with $N = 14$. It is demonstrated that deeper groove leads to higher LDOS with the different characteristics between upper and lower resonant are similar to the case given in Fig. 2. In the mean time, the LDOS can be further enchanced by increasing the number of teeth as exemplified in Fig. 3b for $N = 20$ and $g = 100\ nm$.

To characterize further the corresponding LDOS, we plot the highest value of LDOS at a specific point $(r_0)$ along the line in the middle of the uncorrugated area for both resonant cases. According to Fig. 2 and Fig. 3, it should be noted that these values are not the highest LDOS of the corresponding asymmetric WG. However, it can be used to describe the dynamical characteristics of LDOS with respect to the variation of $g$ and $N$.

Given in Fig. 4a is the variation of LDOS as a function of $g$ at the specific aforementioned point. It is shown that for lower resonant case the related LDOS is increasing monotonously. But this is not the case for the upper case which have the maximum value at $g = 100\ nm$. This remarkable characteristic can be explained as a consequence of LDOS localization for the upper resonant case is mostly in the uncorrugated area, which is getting smaller for increasing groove depth. On the other hand, the variation of number of teeth $N$ shares the same monotonous enhancement of LDOS between both resonant cases as expected.

## 5. SUMMARY

We have discussed the LDOS of an asymmetric waveguide at resonant states of photonic band gap edges. We observed different characteristics between LDOS at upper and lower resonant wavelengths. For upper resonant the corresponding

LDOS is localized in the uncorrugated area, while for the lower resonant is in both corrugated and uncorrugated areas. It is demonstrated that the larger number of teeth as well as deeper groove lead to the enhancement of LDOS.

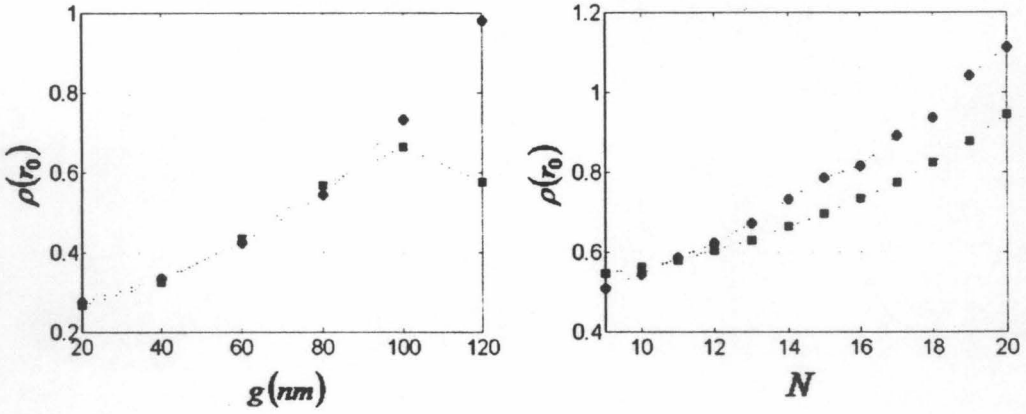


(a) (b)

Fig. 4 Highest LDOS value at specific point along a line in the middle of asymmetric WG for (a) various $g$ with $N = 14$, (b) various $N$ with $g = 100\,nm$.

## 6. ACKNOWLEDGMENT

This work is funded by "Hibah Kompetensi" of year 2014 from the Directorate of Higher education, Ministry of National Education and Culture, Republic of Indonesia. The author would like to thank M. O. Tjia and A. A. Iskandar from Institut Teknologi Bandung, Indonesia, for fruitful discussions.

## 7. REFERENCES

[1] Hopman, W. C. L., Pottier, P., Yudistira, D., Van Lith, J., Lambeck, P. V., De La Rue, R. M., Driessen, A., Hoekstra, H. J. W. M., and de Ridder, R. M., "Quasi-one-dimensional photonic crystal as a compact building block for refractometric optical sensors," IEEE J. Sel. Top. Quantum Electron. 11, 11–16 (2005).

[2] Joannopoulos, J. D., Meade, R., and Winn, J., [Photonic Crystals] Princeton University Press, New Jersey, (1995).

[3] Alatas, H., Iskandar, A. A., and Tjia, M. O., "Structure dependent variations of group velocity, energy loss and confinement in a regular grated waveguide", J. Nonlin. Opt. Phys. Mater. 21, 1250009-1 (2012).

[4] Nikolaev, I. S., Vos, W. L., and Koenderink, A. F., "Accurate calculation of the local density of optical states in inverse-opal photonic crystals," J. Opt. Soc. Am. B 26, 987-997 (2009).

[5] Asatryan, A., Fabre, S., Busch, K., McPhedran, R., Botten, L., de Sterke, M., and Nicorovici, N. A., "Two-dimensional local density of states in two-dimensional photonic crystals," Opt. Express 8, 191-196 (2001)

[6] Paulus, M., Gay-Balmaz, P., and Martin, O. J. F., "Accurate and efficient computation of Green's tensor for stratified media," Phys. Rev. E 62, 5797–5807 (2000).

[7] Elson, J., and Halterman, K., "Local density of states analysis of surface wave modes on truncated photonic crystal surfaces with nonlinear material," Opt. Express 12, 4855-4863 (2004).